Analysis of Microscopic Parameters of Single-Particle Trajectories in Neurons

V. M. Burlakov,[†‡§] R. Taylor,[†] J. Koerner,[†] and N. Emptage[†*]
[†]Department of Pharmacology and [‡]Department of Materials, Oxford University, Oxford, United Kingdom; and [§]Institute for Spectroscopy, Russian Academy of Sciences, Troitsk, Moscow, Russia

ABSTRACT We performed a comparative study of the statistical uncertainties that arise when calculating the velocity and diffusion coefficients from single-particle trajectories. We show that a method where particle mean displacement is used to calculate velocity and mean square fluctuation is used to calculate diffusion coefficient offers greater accuracy than analysis of time-dependent mean square displacement. Our assessment of the performance of the two analysis strategies is conducted in two ways. First, we apply each of the methods to simulated trajectories where each parameter term is known. Second, we analyze the motion of previously uncharacterized EphB2 receptors in the membrane of hippocampal neurons. We find that EphB2 receptors display different types of motion mode and transition between these modes. We present our data as a distribution of microscopic diffusion coefficients for each particle trajectory, which we refer to as partial distributions. Partial distributions are summed to form a cumulative distribution of diffusion coefficients for EphB2 receptors in hippocampal neurons. The structure and interpretation of the EphB2 cumulative distribution are discussed.

INTRODUCTION

Single-particle tracking (SPT) is a powerful tool with which to study protein receptor movement in living neurons (1–8). The approach measures the position of a particle (a quantum dot or fluorescent dye molecule attached to a receptor (1)) at discrete time increments. A trajectory is produced by expressing the coordinates of particle position as a function of time. Analysis of the trajectory can then be used to reveal parameters that characterize different types of particle motion. These include simple diffusion, diffusion with directed flow, corralled motion, and anomalous diffusion (2,9,10). There are two main approaches used in the analysis of particle trajectories (11), the most popular of which measures the mean square displacement (MSD) of a particle as a function of time. To extract the diffusion coefficient, D, and flow velocity, V, from the function MSD(t), an assigned function that characterizes a specific motion mode is required. Thus, an a priori decision is necessarily taken about the type of motion observed within a trajectory. The values returned for D and V represent the characteristic parameters of the MSD(t) curve and contain information about all interactions within the selected time window. An alternative approach applies analysis of particle mean displacement (MD) for the determination of V and the mean square fluctuation (MSF) for determination of D. Here, microscopic values of D and V are obtained for the shortest measured timescale, specifically, the time interval between data point acquisitions. One consequence of this is that the determination of D is accurate as the use of a microscopic timescale does not overrepresent the occurrence of interactions or collisions with obstacles provided that the time interval between collisions is longer than the time interval between data point acquisitions. It is important to note that the approach has a further advantage in that it does not require an a priori decision to be taken about the type of motion but it does have the disadvantage that it provides limited information about corralled motion and/or anomalous diffusion, as these require analysis of particle motion across much longer (macroscopic) timescales.

The results of trajectory analysis are frequently presented as a histogram, where the number of particles within a defined range of D is expressed against D (12–15). In these distributions, each trajectory, or part-trajectory (a period where the particle is within a single motion mode), is characterized by a single value of D. Where a stationary random process (diffusion) accounts for particle motion, any variation of D between different particles should be the same as variations of D for a single particle provided that the particle's trajectory is extensive enough to extend across the space available for all particles (the ensemble average is equal to the time average (16)). In fact, this is rarely the case. Particle motion is frequently recorded across a restricted time interval where the particle trajectory length is too short to fulfill this important caveat. As single particles may experience motion characterized by variable diffusion coefficients (12), variations in instantaneous D have been used for confinement analysis of particle motion (14,15). However, averaging these variations over a particle trajectory, or a trajectory section characterized by a particular motion mode, is likely to result in a loss of information. In an attempt to resolve these issues, we have extended the idea of Saxton (4) and introduce a distribution of microscopic diffusion coefficients for each particle trajectory, which we refer to as a partial distribution. The sum of all partial distributions, a cumulative distribution, can be

Submitted November 8, 2009, and accepted for publication June 1, 2010.

*Correspondence: nigel.emptage@pharm.ox.ac.uk

Editor: Denis Wirtz.

0006-3495/10/09/1368/9 $2.00

doi: 10.1016/j.bpj.2010.06.021

considered as characteristic of the entire cell under the specific conditions of the data acquisition.

To obtain a measure of the reliability of our distributions, we performed a systematic assessment of trajectory analysis made with MSD(t) and MD-MSF algorithms against simulated data, with defined terms for D and V. We show that the MD-MSF approach is more accurate for the same length of particle trajectory. Applying the MD-MSF method to experimental trajectories of EphB2 receptors we find that the cumulative distribution of D exhibits an interesting structure that is not resolved by the MSD(t) approach.

This article is organized as follows. Algorithms for calculating D and V are given for the MD-MSF and MSD (t) analysis methods. We present an analysis of statistical uncertainty for each approach. We give examples of determination of trajectory parameters from a complex simulated trajectory and introduce partial distributions $f(D)$ and $f(V)$. Finally, we describe analysis of experimental trajectories of EphB2 receptors in hippocampal neurons and present a cumulative distribution of D values.

RESULTS

Algorithms for analyzing particle trajectories

To illustrate the calculation procedure for MSD(t) and MD-MSF, consider a trajectory given by the sequence of N successive particle positions $x_i = x(i\delta t)$ and $y_i = y(i\delta t)$, $i = 1,2,\ldots N$, where $\delta t$is the time step in particle position recording. The function MSD(t) is calculated as (11,17)

$$MSD(n\delta t) \equiv \langle r^2(n\delta t)\rangle = \langle x^2(n\delta t)\rangle + \langle y^2(n\delta t)\rangle = \frac{1}{N-n-1}\sum_{i=1}^{N-n-1}\left[(x_{i+n}-x_i)^2+(y_{i+n}-y_i)^2\right]. \quad (1)$$

To obtain the diffusion coefficient, D, and velocity, V, the function is approximated as

$$MSD(n\delta t) = 4Dn\delta t + V^2(n\delta t)^2, \quad (2)$$

using D and V as fit parameters. We restrict our consideration to cases of simple diffusion and diffusion with flow. Two examples of the MSD(t) function calculated from simulated trajectories with $V = 0$ and $D = 0.3\ \mu m^2/s$ are shown in Fig. 1. Although both trajectories in Fig. 1 are generated with $V = 0$, the least-square fit of the MSD returns some nonzero V^2 values, one of which (curve 2) is negative. In the analysis, such negative values are necessarily disregarded.

In contrast with the MSD(t) approach, the MD-MSF approach returns the values of V_x and V_y alongside D according to the equations

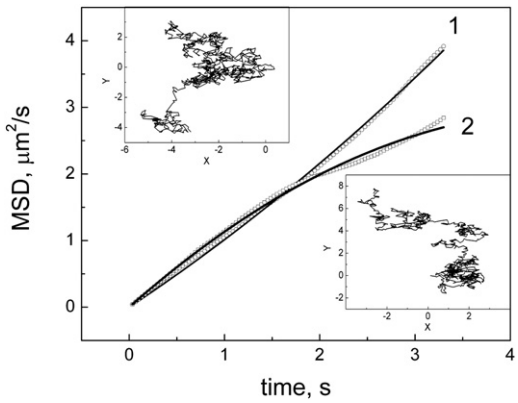

FIGURE 1 Mean square displacement is plotted as a function of time (*symbols*) for two simulated trajectories (*insets*). The trajectories were simulated with $D_{in} = 0.3\ \mu m^2/s$ and $V = 0$. Solid lines show the least-square approximations obtained using Eq. 2. Curve 1 has positive curvature, which, according to Eq. 2. means that $V^2 > 0$, whereas curve 2 shows negative curvature, indicating that $V^2 < 0$.

$$V_x = \frac{\langle x(\delta t)\rangle}{\delta t} = \frac{(x_N - x_1)}{(N-1)\delta t},\quad V_y = \frac{\langle y(\delta t)\rangle}{\delta t} = \frac{(y_N - y_1)}{(N-1)\delta t},$$
$$D = \frac{1}{4(N-1)\delta t}\times\sum_{i=1}^{N-1}\left[(x_{i+1}-x_i-V_x\delta t)^2+(y_{i+1}-y_i-V_y\delta t)^2\right]. \quad (3)$$

Here, velocity components are determined from MD over the time step δt, whereas the diffusion coefficient is derived from the MSF about the mean value for the same time step. Therefore, values of D and V obtained using the MD-MSF approach (equivalent to the velocity analysis discussed in Qian et al. (11)) characterize particle dynamics on a far shorter timescale, δt, than those obtained using the MSD (t) approach that relate to the timescale $n\delta t$ (usually with $N >> n >> 1$). The values returned by Eq. 3 provide microscopic parameters that characterize particle motion on the short timescale, δt. Therefore, any individual parameter will only occasionally be influenced by the occurrence of a rare event such as an interaction with an obstacle when obstacles are sparse. The use of a shorter timescale will allow better statistical averaging for the same trajectory domain. As can be seen from Eq. 1, MSD($n\delta t$) is calculated by averaging over $N - n - 1$ points, many of which are statistically dependent (4,11). This can result in a higher statistical uncertainty in the V and D values, an issue that is analyzed in the next section.

Statistical uncertainties of the MSD(t) and MD-MSF approaches

To assess the statistical accuracy of the MSD(t) and MD-MSF approaches, we simulated a large number ($>10^5$) of particle trajectories and gave them the same input parameters, V_{in} and D_{in}. Each trajectory was generated using a

continuous diffusion model by summing the random displacements and directed motion with a given velocity, as described in Saxton (3). Each random displacement in a trajectory consists of 20 random steps. The term random displacement is used for particle displacement during the acquisition time step, whereas the term random step is related to a hypothetical molecular step performed during molecular mean free time. The choice of only 20 random steps in each random displacement is made to mimic realistic statistics of random displacement on one hand, and for the sake of computational efficiency on the other hand, and has no influence on the values and uncertainty of kinetic coefficients. From each simulated trajectory containing $N = 10^3$ points, we calculated the values of D and V applying both analytical approaches, and the ensembles of all calculated values were represented in the form of distributions $f(D)$ and $f(V)$. It is worth noting that although the MD-MSF method returns velocity components V_x and V_y to ease comparison with MSD(t), we present the total velocity, $V = \sqrt{V_x^2 + V_y^2}$. The distributions $f(D)$ and $f(V)$ are shown in Fig. 2 for two sets of input parameters: 1), $D_{in} = 0.3\ \mu m^2/s$, $V_{x,in} = V_{y,in} = 0$; and 2), $D_{in} = 0.3\ \mu m^2/s$, $V_{x,in} = V_{y,in} = 1/\sqrt{2}\ \mu m/s$, and for two values of the maximum time lag, $n\delta t$, for the MSD(t) method (Eq. 2), $n = 10$ and $n = 100$.

Fig. 2 *a*, curve 1, reveals that the accuracy is highest in the determination of D, illustrated by the narrowest distribution $f(D)$, when determined by the MD-MSF method (Eq. 3). In Fig. 2 *a*, curves 2 and 3 are obtained for values of D calculated using the MSD method (Eqs. 1 and 2) with $n = 10$ and $n = 100$, respectively. The figure clearly illustrates that the accuracy in determination of D increases as the time interval used for its calculation falls, in agreement with Saxton (4). The effect of the maximum time lag is opposite when applied to velocity distributions, as shown in Fig. 2 *b*. Here, the result is strongly dependent upon the input velocity. For $V_{in} = 0$, the distribution $f(V)$ obtained with the MSD(t) method with $n = 100$ (curve 3) is significantly narrower than that obtained with $n = 10$ (curve 2). However, the narrowest distribution is again obtained by MD-MSF method (curve 1). The extent to which the choice of algorithm is important decreases sharply with increased input velocity (compare curves 4–6). As one can see from Fig. 2 *b*, curves 1–3, the maxima in $f(V)$ for $V_{in} = 0$ are shifted with respect to V_{in}. This indicates a systematic error in determining velocity in two dimensions. A more accurate value for the velocity can be obtained by calculating the components V_x and V_y (18) (corresponding software (Java applet) is available on request from V. M. Burlakov (victor.burlakov@materials.ox.ac.uk)). and analyzing their distributions, as illustrated by Eq. S6 in the Supporting Material and shown in Fig. 2 *b*, curve 7.

Our results obtained by direct calculation indicate that the MD-MSF approach outperformed the estimates presented in Saxton (11). However, to gather further confidence in the utility of the approach, we performed calculations of the distributions similar to those shown in Fig. 2 for trajectories with different numbers of points, $N = 250$–$15{,}000$. In each instance, the distribution we calculated for the parameter values contained 96% of the total probability distribution, i.e., 96% confidence interval for ΔD_{96} and ΔV_{96}. The normalized confidence intervals $\Delta D_{96}/D_{in}$ and $\Delta V_{96}/V_2$ are presented in Fig. 3 as functions of N. We used the value $V_2 = \sqrt{4D_{in}/\delta t}$ for normalization because the flow displacement $V\delta t$ could also be treated as a random displacement $\sqrt{4D_{in}\delta t}$, which gives the amplitude V_2 for the uncertainty. Note that for the parameter values $D_{in} = 0.3\ \mu m^2/s$ and $\delta t = 0.033$ the value of V_2 is ~6 μm/s. We found that for all N values, the MD-MSF method produces the least uncertainty for both D and V. The relative width of the confidence interval in Fig. 3 *a* scales as

$$\Delta D_{96}/D_{in} = A \times N^{-1/2}, \quad (4)$$

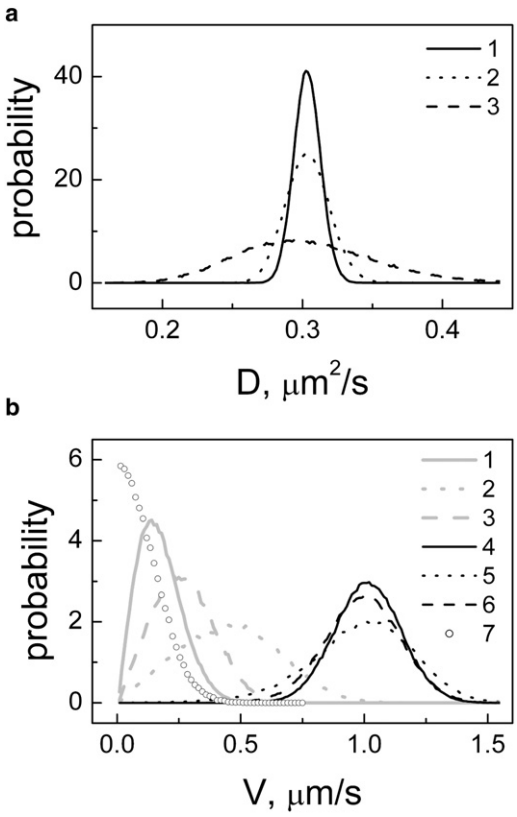

FIGURE 2 The probability distribution for the diffusion coefficients, D (*a*), and velocities, V (*b*), obtained from 10^5 simulated trajectories, each of 1000 points, determined by the MD-MSF and MSD(t) methods. Curves 1 in *a* and 4 and 7 in *b* were obtained using the MD-MSF method. Curves 2 in *a* and 5 in *b* ($n = 10$) and curves 3 in *a* and 6 in *b* ($n = 100$) were obtained by the MSD(t) method. Trajectories were simulated using two sets of input parameters: $D_{in} = 0.3\ \mu m^2/s$, $V_{x,in} = V_{y,in} = 0$ (curves 1–3 and 7 in *b*) and $D_{in} = 0.3\ \mu m^2/s$, $V_{x,in} = V_{y,in} = 1/\sqrt{2}\mu m/s$ (curves 2–4 in *b*). The data presented in *a* do not depend on velocity values. Curve 7 in *b* shows half of the probability distribution for $V_x = V_y > 0$ obtained by the MD-MSF method.

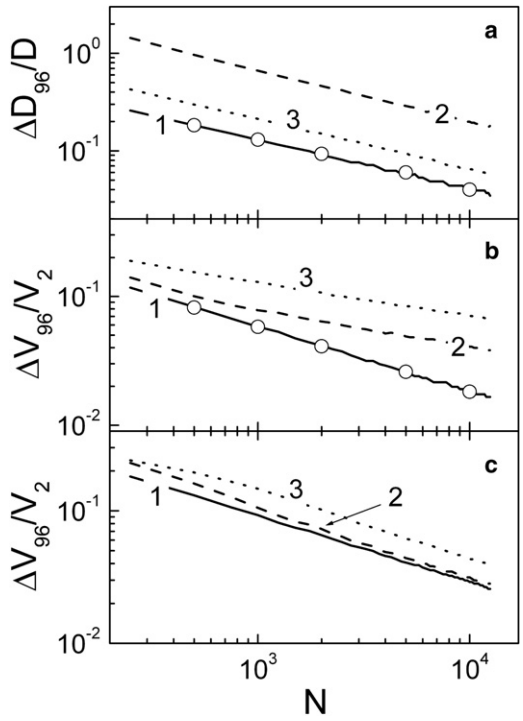

FIGURE 3 The relative uncertainties (96% confidence intervals) for the diffusion coefficients, D (*a*), and velocities, V (*b* and *c*), plotted as a function of the number of points, N. Curves 1 were obtained using MD-MSF, whereas curves 2 and 3 were obtained using the MSD(t) method with $n = 10$ and 100, respectively. Curves in *a* and *b* were calculated for $D_{in} = 0.3\ \mu m^2/s$, $V_{x,in} = V_{y,in} = 0$ and those in *c* for $D_{in} = 0.3\ \mu m^2/s$, $V_{x,in} = V_{y,in} = 1/\sqrt{2}\mu m/s$.

where $A = 4.0$ for curve 1, $A = 6.6$ for curve 2, and $A = 21.0$ for curve 3. The curves in Fig. 3 *b* are best approximated by the function $\Delta V_{96}/V_2 = B \times N^{-\alpha}$, where $B = 1.85$, 0.78, and 0.65 and $\alpha = 0.5$, 0.26, and 0.3 for curves 1–3, respectively. For the curves in Fig. 3 *c*, we found the best approximations with the parameters $C = 2.9$ and 4.6 and $\alpha = 0.5$ and 0.5 for curves 1 and 2, respectively. Numerical results on the uncertainties in calculating V and D using MD-MSF are in excellent agreement with those obtained analytically (see Supporting Material), as indicated by the symbols in Fig. 3, *a* and *b*.

In summary, we find that the statistical accuracy of the MD-MSF method is higher than that of MSD(t). The accuracy of the MSD(t) method in obtaining D generally increases as that for V decreases when decreasing the maximum time lag. We find that statistical fluctuations of D and V (for $V_{in} = 1.0\ \mu m/s$) decrease in accordance with the square root of the number, N, of statistically independent values used for averaging. To achieve accuracy of $\pm 6.5\%$ in the determination of D using the MD-MSF approach, N should be 1000. To achieve comparable accuracy using the MSD(t) approach with $n = 100$, N has to exceed 15,000. As our experimental trajectories contain ~6000 points, the maximum accuracy in obtaining a single D value with the MSD(t) approach would be $\pm 15\%$. Detection of variations in D within a single trajectory would impose a limit on the number of points: were this around $N = 1000$, the accuracy of the MSD(t) method (with $n = 100$) would approach not better than $\pm 30\%$. The accuracy of obtaining V by the MD-MSF approach with $N = 1000$ is $> \pm 5\%$, comparable to that using the MSD(t) method with $n = 100$. An accuracy of 5% in calculating velocity is given relative to V_2, which for $D = 0.1\ \mu m^2/s$ amounts to $V_2 = 3.5\ \mu m/s$, resulting in an absolute accuracy of about $\pm 0.2\ \mu m/s$.

Applying the MSD(*t*) and MD-MSF approaches to complex trajectories

Here, we illustrate the level of accuracy in the determination of D and V from a single trajectory using the MSD(t) and MD-MSF methods. A simulated complex trajectory containing $M = 10^5$ particle coordinates consists of five sections of equal length with different values of D_{in} and V_{in} (Fig. 4, *a* and *b*, *black lines*). A single pair of D and V values is calculated from each trajectory segment containing 1000 particle positions. Starting with the first 1000 points, the segment has been slid along the trajectory one point at a time, and the values of D and V corresponding to each of the time increments are calculated. The results are then used to obtain distributions $f(D)$ and $f(V)$ (Fig. 4, *c* and *d*).

In Fig. 4 *a*, the values of D fluctuate about the input value, D_{in}. The fluctuation amplitude is higher for the blue curve (MSD(t)) than for the red one (MD-MSF). The large fluctuations of D obtained by the MSD(t) method produces a broad $f(D)$ distribution (Fig. 4 *c*) that fails to show peaks around the D_{in} values (*sharp black lines*), whereas the distribution obtained by the MD-MSF method shows distinct peaks around the D_{in} values. These results are in good agreement with the distributions shown by curves 1 and 3 of Fig. 2 *a*. In the determination of V, large fluctuations are observed in both methods (Fig. 4 *b*). The corresponding $f(V)$ distributions (Fig. 4 *d*) show a modest correlation with the input distribution (*sharp black lines*) for V values $<0.6\ \mu m/s$, whereas the peaks at $V = 1\ \mu m/s$ report V correctly and with comparable accuracy for both methods. Again, this correlates with the distributions shown in Fig. 2 *b* (see curves 4 and 6).

Our experimental trajectories are typically 6000 points. Therefore, it was important to check that the approach previously applied to long trajectories also works for a shorter trajectory. To assess this, in the determination of D and V we performed a simulation, the results of which are presented in Fig. 5. The simulated trajectory consists of three sections with different V_{in} and D_{in} values (Figs. 5, *a* and *b*, *black lines*). The corresponding distributions are shown in Fig. 5, *c* and *d*, with the input values indicated by sharp black lines. It is interesting that even for these short trajectories the MD-MSF method achieves a good

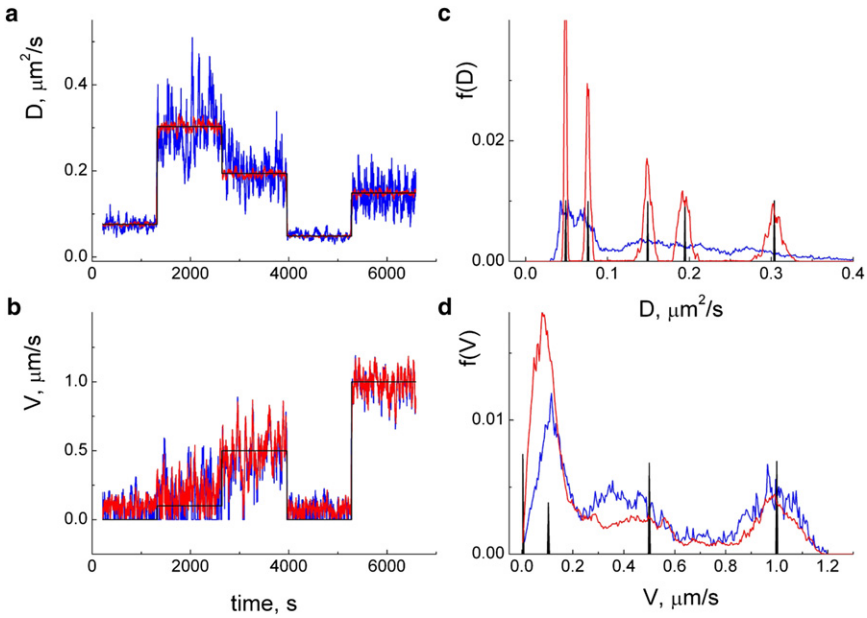

FIGURE 4 Time-dependent diffusion coefficients, D (*a*), velocity, V (*b*), $f(D)$ distributions (*c*), and $f(V)$ distributions (*d*) are calculated for a simulated trajectory containing 10^5 points using the MD-MSF (*red lines*) and MSD(t) (*blue lines*) methods. The parameters for each time point were calculated from MD, MSD, and MSF by averaging over $N = 1000$ trajectory points. Black lines indicate the input parameter values.

determination for each value of D. This is in contrast to the MSD(t) method, where the determination of D produces values that are displaced and spread, with the highest value of D, $D_{\text{in}} = \sim 0.3\ \mu\text{m}^2/\text{s}$, remaining completely unresolved. In the determination of V, neither method is exceptionally good under these conditions, but the MD-MSF method does perform slightly better, as seen in Fig. 5 *d*.

Many of the parameter values calculated for sliding trajectory segments are correlated. This correlation can be calculated directly as $F(m) = 1/M - m\sum_{i=1}^{M-m}(D(i\delta t + m\delta t) - D_{in}) \times (D(i\delta t) - D_{in})$, where $F(m)$ is the correlation function. Our numerical analysis and the results of Saxton (11) indicate that correlation between D values decreases as $F(m) = 1 - m/N$ for $m < N$ and remains close to zero for $m > N$. This means that the number of statistically independent parameter values is equal to the number of nonoverlapping segments contained in the trajectory. Using parameter values from overlapping segments in the distributions $f(D)$ and $f(V)$ results in smoother curves but is unlikely to increase the information content in these distributions.

In summary, we demonstrate that with the MD-MSF method it is possible to reconstruct with reasonable accuracy the time variation of diffusion coefficient and velocity

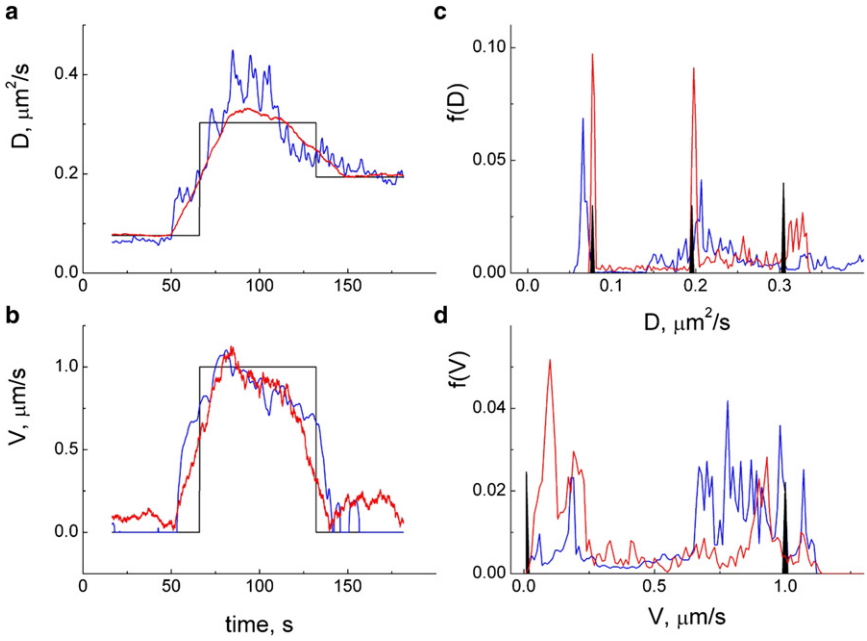

FIGURE 5 Same as for Fig. 4, but calculated for a short trajectory containing 6000 points.

within a particle trajectory. The accuracy of the reconstruction is higher with lower rates of variation of D and V, or when there are a large number of trajectory points with quasiconstant parameter values. For experimental trajectories, this means that high data acquisition rates will be beneficial. Arrays of D and V values obtained from a single trajectory are conveniently represented in the form of distributions $f(D)$ and $f(V)$.

Analysis of the quantum-dot-labeled EphB2-Receptor motion

In the final section of this work, we perform a trajectory analysis on a previously uncharacterized neuronal membrane receptor, the EphB2 receptor. EphB2 receptors belong to a family of receptor tyrosine kinases, which, along with their membrane-bound ligands, the Eph receptor interacting proteins (ephrins), are involved in a wide variety of signaling processes both outside and within the central nervous system (19,20). All Eph receptors are transmembrane proteins with highly conserved extra- and intracellular domains. A remarkable feature of these receptors is that bidirectional signaling can be initiated upon binding to ephrin (21,22).

We label and track EphB2 receptors in the membrane of hippocampal neurons using quantum dots (QDs) linked to antibodies targeted to the extracellular domain of the EphB2-receptor. Specificity of labeling was confirmed by colocalization of EphB2-R-QDs and EphB2-R-YFP hybrid proteins. EphB2-R-QDs are treated as a single EphB2-R-QD complex when blinking is observed. The localization of EphB2-QD puncta to dendritic processes is shown in Fig. 6 *A*. Initial analysis of EphB2-R-QD movement reveals different types of motion, where some receptors are relatively static while others diffuse over large distances within the dendrites. These patterns are readily observed in a projection image of 6000 image frames of 33 ms each (Fig. 6 *B*). The patterns of EphB2-R-QD movement observed appear similar to a variety of previously studied neuronal membrane receptors (7,14,15,17,19,23,24).

Application of the MD-MSF method to the analysis of EphB2-R-QD motion reveals an additional feature of EphB2-QD movement: receptors can transition between motion modes. Detection of these transitions is achieved without user intervention, that is, no parsing of the data takes place before the analysis is conducted. Examples of six trajectories are presented in Fig. 7. Despite the anisotropic form of these trajectories, the analysis shows that the particle velocity in all cases fluctuates around zero, indicating that the movement represents random motion of the receptors. Following the analysis approach outlined earlier, we compute distributions $f(D)$ for each trajectory, which we call partial distributions (PDs), calculated using $N = 1000$ to ensure that the structure of $f(D)$ is not due to statistical fluctuations of D. Fig. 8 shows PDs calculated for each of the trajectories presented in Fig. 7 with both the MSD(t) and MD-MSF analysis methods applied. One can see that the PDs obtained using the two methods can differ markedly from one another. The most prominent variation is observed for PDs corresponding to the trajectory shown in Fig. 7 *b*. This trajectory shows highly restricted motion for the MSD(t) approach, resulting in a low D value. In contrast, the MD-MSF method returns relatively high values of D, suggesting large-amplitude random fluctuations of the

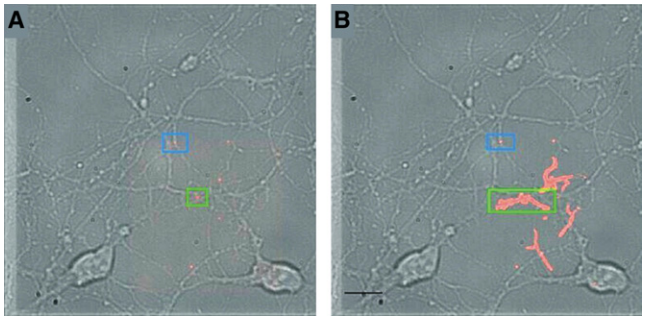

FIGURE 6 QD images are overlain onto a transmitted light image of cultured hippocampal neurons. The image shows QD-labeled EphB2-receptors (*red*) for both a single frame (*A*) and a maximum intensity projection of 6000 frames (*B*). Receptors have both localized trajectories (*blue rectangles*) and trajectories that extend over large distances (*green rectangles*). Scale bar, 10 μm.

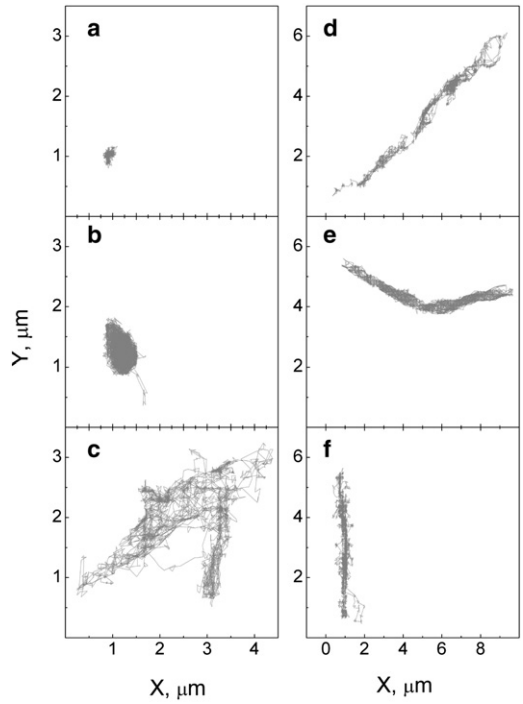

FIGURE 7 Experimental trajectories of QD-labeled EphB2-receptors in hippocampal neurons consisting of 6000 particle position points acquired at a frequency of 30 Hz. These trajectories illustrate localized and restricted motion (*a–c*) and highly anisotropic delocalized motion (*d–f*).

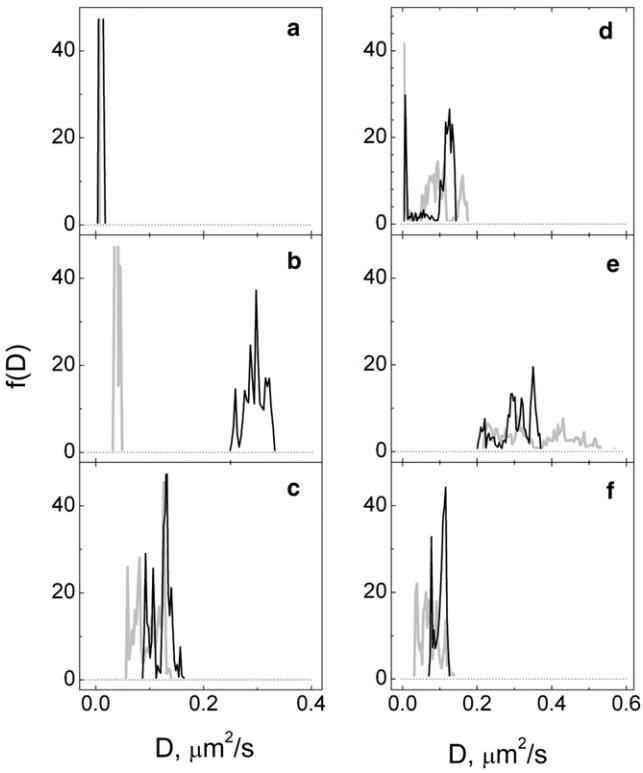

FIGURE 8 Distributions of diffusion coefficients, $f(D)$, obtained for trajectories *a–f* in Fig. 7 using MSD(t) (*gray*) and MD-MSF (*black*) methods for $N = 1000$ and $n = 100$. All distributions are normalized on 1.

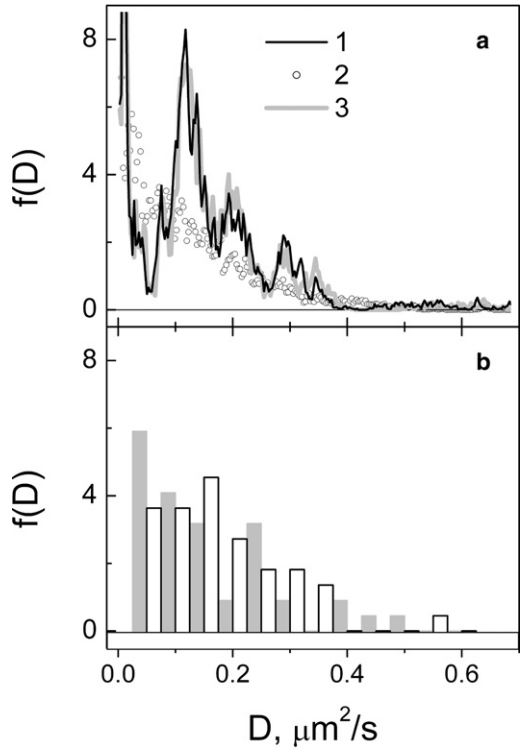

FIGURE 9 (*a*) The cumulative distribution of diffusion coefficients, $f(D)$, from the normalized sum of 44 individual distributions obtained for $N = 1000$ using the MD-MSF (*black*) and MSD(t) method with $n = 100$ (*open circles*) and the MSD(t) method with $n = 3$ (*gray*). (*b*) The distribution histogram of diffusion coefficients obtained by calculating a single average diffusion coefficient for each of the 44 trajectories. Results obtained using the MD-MSF method are shown by open bars, and those obtained using MSD(t) with $n = 100$ are shown by gray bars.

particle. This analysis outcome underscores the conclusions drawn from the simulations presented in the preceding sections, where it is shown that MD-MSF delivers reliable information about particle dynamics on the timescale of δt, and is insensitive to interactions producing restricted motion across longer timescales. It is not surprising, therefore, that the cumulative distribution $f(D)$ obtained using the MD-MSF method is entirely different from that obtained using the MSD(t) method (Fig. 9 *a*). The distribution shown with curve 1 is obtained using the MD-MSF method and displays a complex structure. This structure is partially reproduced in curve 2, obtained using MSD(t) with $n = 3$, and is completely absent in distribution curve 3, obtained using the MSD(t) method with $n = 100$. The distribution seen in curve 3 resembles that obtained when only a single value of D is calculated from each trajectory (Fig. 9 *b*). Here, the histograms are similar and lack structure irrespective of the method used for calculating D. Fig. 9 *b* clearly illustrates the extent to which information is lost by unnecessary averaging, i.e., assigning each particle trajectory (or fraction of a trajectory within a single motion mode) to a single value of D.

One can also plot a cumulative distribution for velocity, $f(V)$, to characterize the active motion of particles. Fig. 10 shows the $f(V)$ distributions corresponding to the $f(D)$ distributions in Fig. 9 *b*. According to the distribution obtained using the MD-MSF method (curve 1), the particle velocities are scattered around zero. The distribution obtained using the MSD(t) method with $n = 100$ (curve 2) shows that particle velocities are spread in the region between 0 and 0.5 μm/s, suggesting on average the presence of directed motion. An even larger spread of particle velocities, from 0 to 1.5 μm/s, is found in the distribution obtained using MSD(t) with $n = 3$ (curve 3). A comparison of the distributions in Figs. 9 *a* and 10 shows that the most reliable way of calculating both D and V values simultaneously is to use the MD-MSF approach. We believe that the structures in $f(V)$ produced by the MSD(t) method are artifacts, as their form changes with the number n; therefore, we focus our discussion on the structures of $f(D)$ shown in Figs. 8 and 9 *a*, respectively.

DISCUSSION

We have performed a comparative study of the degree of uncertainty that arises when calculating kinetic coefficients from SPT data by two analysis methods: One is a commonly used method based on time-dependent mean square

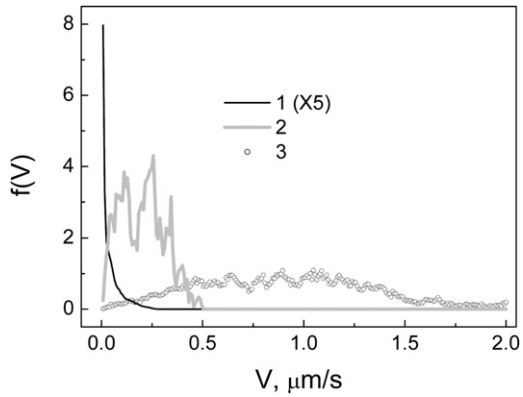

FIGURE 10 The cumulative distribution for velocity, $f(V)$, from the normalized sum of 44 individual distributions. The cumulative distributions of velocities from the normalized sum of 44 individual distributions obtained for $N = 1000$ using the MD-MSF method (*black*) and MSD(t) method with $n = 100$ (*gray*) and MSD(t) with $n = 3$ (*open circles*). The scale of y axes for curve 1 should be multiplied by a factor of 5.

displacement, MSD(t), whereas the other is a method where particle velocity is calculated using the MD, and diffusion coefficient is calculated from mean the MSF. We show that for free diffusion and diffusion with flow, the MD-MSF method is consistently more accurate than the MSD(t) method. This is most evident when seeking to determine particle diffusion coefficient and flow velocity simultaneously. In contrast, where anomalous diffusion or corralled motion are to be examined, the MSD(t) method is a more appropriate choice. Applying the MD-MSF method to a segment sliding along a trajectory allows one to obtain the time dependence of D and V, thereby increasing information about particle dynamics. The time-dependent values of D and V can be translated into PDs for an individual particle trajectory. The sum of the PDs for many particles provides a method where information about the general performance of a receptor type, in this case EphB2, may be provided for a given cell type under given conditions.

Many PDs reveal rather a wide range of D values, with some illustrating a change in motion mode, such as that seen in Fig. 8 *d*, that contains two peaks at $D \approx 0$ and $D \approx 0.1\ \mu m^2/s$. The distributions shown in Fig. 8, *a* and *c*, show peaks at low values, $D << 0.05\ \mu m^2/s$, and peaks at much higher values, $D > 0.1\ \mu m^2/s$. The former represents localized or restricted motion. For this category of motion, one might speculate that the receptors are corralled or tethered at a synapse. Clear precedents exist where low diffusion coefficient is correlated with synaptic localization, for example, for glycine receptors (5). How might trapping of EphB2 receptors be achieved? A number of possibilities can readily be envisaged. First, the protein content of a specific membrane compartment may be high. This is particularly true of synapses. When the protein content of the membrane is high, diffusing particles have a high collision rate with proteins, reducing the diffusion coefficient. Second, the cytoskeletal architecture of neurons is known to be regionally specialized, in particular at the synapse. As the polymerization status of cytoskeletal proteins can influence diffusion of proteins within the membrane (15,25), the diffusion coefficient may be reduced at regions of specialization. Third, EphB2-receptors are known to interact with glutamatergic receptor interacting protein 1 (GRIP1), a synaptic scaffolding protein (26). The physical tethering of receptors to proteins such as GRIP1 will likely have an impact on the diffusion coefficient. Finally, differences in lipid composition of the membrane, in particular subdomains such as lipid rafts, are known to influence the diffusion coefficient of proteins in the membrane (10) and may influence the movement of EphB2 receptors.

There are clear examples of EphB2 motion that could be assigned as showing normal diffusion but in fact have a time-dependent diffusion coefficient (see Figs. 7, *a* and *e*, and 8, *c* and *e*). This pattern is evident for many of the trajectories. A broad range of values for D can be seen in the cumulative $f(D)$ distribution (Fig. 9 *a*) obtained by summing the distributions (44 in total) of individual trajectories. The cumulative distribution obtained using MSD(t) method lacks structure, whereas that produced with the MD-MSF approach shows distinct peaks. The largest and narrowest peak is at $D = 0.12\ \mu m^2/s$. One can identify also two smaller and broader peaks at ~$0.2\ \mu m^2/s$ and $0.3\ \mu m^2/s$. At this time, we have no explanation for this structure, although there are a number of interesting possibilities. One way of explaining the peaks in Fig. 9 *a* would be to assume that membrane and cytoskeletal compartments differentially affect particle diffusion. Another possibility is to assume that there are specific mechanisms that influence the microscopic diffusion coefficient, and that these may arise from a direct interaction of the EphB2 receptor with proteins within the cell. EphB2-receptors are known to interact with actin (REF) and GRIP1 (22) or may be an indirect consequence of cytoskeletal interactions with other membrane proteins. It is clear that further work will need to be conducted to identify the basis of the structure seen in the cumulative distribution.

In conclusion, our study describes a method (MD-MSF) for analyzing single-particle trajectories by which more complete information about particle dynamics is extracted than using the commonly applied method, MSD(t). However, although powerful for the determination of D and V, the MD-MSF approach does not supersede, but complements, the MSD(t) method, as the latter approach is more appropriately applied when studying the constrained motion of particles. We have used the MD-MSF method to study the EphB2 receptor motion in hippocampal neurons and show that the cumulative distribution of diffusion coefficients has a complex structure. The biological basis of this structure and whether it is observed for other classes of membrane receptor remains to be explored.

SUPPORTING MATERIAL

Methods and additional references are available at http://www.biophysj.org/biophysj/supplemental/S0006-3495(10)00733-2.

We sincerely thank Laura Andreae, who provided us with invaluable assistance in establishing QD labeling, and Bernhard Seiser for converting the Fortran code to Java applet.

V.M.B. gratefully acknowledges the support of the EPSRC, BBSRC, and MRC under the Discipline Hopping Award Scheme. R.T. and N.J.E. thank the MRC for support.

REFERENCES

1. Saxton, M. J., and K. Jacobson. 1997. Single-particle tracking: applications to membrane dynamics. *Annu. Rev. Biophys. Biomol. Struct.* 26:373–399.
2. Kusumi, A., Y. Sako, and M. Yamamoto. 1993. Confined lateral diffusion of membrane receptors as studied by single particle tracking (nanovid microscopy). Effects of calcium-induced differentiation in cultured epithelial cells. *Biophys. J.* 65:2021–2040.
3. Saxton, M. J. 1994. Single-particle tracking: models of directed transport. *Biophys. J.* 67:2110–2119.
4. Saxton, M. J. 1997. Single-particle tracking: the distribution of diffusion coefficients. *Biophys. J.* 72:1744–1753.
5. Dahan, M., S. Lévi, …, A. Triller. 2003. Diffusion dynamics of glycine receptors revealed by single-quantum dot tracking. *Science.* 302: 442–445.
6. Courty, S., C. Bouzigues, …, M. Dahan. 2006. Tracking individual proteins in living cells using single quantum dot imaging. *Methods Enzymol.* 414:211–228.
7. Echarte, M. M., L. Bruno, …, L. I. Pietrasanta. 2007. Quantitative single particle tracking of NGF-receptor complexes: transport is bidirectional but biased by longer retrograde run lengths. *FEBS Lett.* 581:2905–2913.
8. Triller, A., and D. Choquet. 2008. New concepts in synaptic biology derived from single-molecule imaging. *Neuron.* 59:359–374.
9. Sako, Y., and A. Kusumi. 1994. Compartmentalized structure of the plasma membrane for receptor movements as revealed by a nanometer-level motion analysis. *J. Cell Biol.* 125:1251–1264.
10. Dietrich, C., B. Yang, …, K. Jacobson. 2002. Relationship of lipid rafts to transient confinement zones detected by single particle tracking. *Biophys. J.* 82:274–284.
11. Qian, H., M. P. Sheetz, and E. L. Elson. 1991. Single particle tracking. Analysis of diffusion and flow in two-dimensional systems. *Biophys. J.* 60:910–921.
12. Bats, C., L. Groc, and D. Choquet. 2007. The interaction between Stargazin and PSD-95 regulates AMPA receptor surface trafficking. *Neuron.* 53:719–734.
13. Haggie, P. M., J. K. Kim, …, A. S. Verkman. 2006. Tracking of quantum dot-labeled CFTR shows near immobilization by C-terminal PDZ interactions. *Mol. Biol. Cell.* 17:4937–4945.
14. Sergé, A., L. Fourgeaud, …, D. Choquet. 2002. Receptor activation and homer differentially control the lateral mobility of metabotropic glutamate receptor 5 in the neural membrane. *J. Neurosci.* 22:3910–3920.
15. Serge, A., L. Fourgeaud, …, D. Choquet. 2003. Active surface transport of metabotropic glutamate receptors through binding to microtubules and actin flow. *J. Cell Sci.* 116:5015–5022.
16. Landau, L. D., and E. M. Lifshitz. 1969. Statistical Physics. Pergamon Press, Oxford, United Kingdom.
17. Lee, G. M., A. Ishihara, and K. A. Jacobson. 1991. Direct observation of Brownian motion of lipids in a membrane. *Proc. Natl. Acad. Sci. USA.* 88:6274–6278.
18. Tardin, C., L. Cognet, …, D. Choquet. 2003. Direct imaging of lateral movements of AMPA receptors inside synapses. *EMBO J.* 22: 4656–4665.
19. Zhou, R. 1998. The Eph family receptors and ligands. *Pharmacol. Ther.* 77:151–181.
20. Klein, R. 2009. Bidirectional modulation of synaptic functions by Eph/ephrin signaling. *Nat. Neurosci.* 12:15–20.
21. Irie, F., and Y. Yamaguchi. 2002. EphB receptors regulate dendritic spine development via intersectin, Cdc42 and N-WASP. *Nat. Neurosci.* 5:1117–1118.
22. Penzes, P., A. Beeser, …, R. L. Huganir. 2003. Rapid induction of dendritic spine morphogenesis by trans-synaptic ephrinB-EphB receptor activation of the Rho-GEF kalirin. *Neuron.* 37:263–274.
23. Groc, L., M. Heine, …, D. Choquet. 2004. Differential activity-dependent regulation of the lateral mobilities of AMPA and NMDA receptors. *Nat. Neurosci.* 7:695–696.
24. Meier, J., C. Vannier, …, D. Choquet. 2001. Fast and reversible trapping of surface glycine receptors by gephyrin. *Nat. Neurosci.* 4:253–260.
25. Charrier, C., M. V. Ehrensperger, …, A. Triller. 2006. Cytoskeleton regulation of glycine receptor number at synapses and diffusion in the plasma membrane. *J. Neurosci.* 26:8502–8511.
26. Contractor, A., C. Rogers, …, S. F. Heinemann. 2002. Trans-synaptic Eph receptor-ephrin signaling in hippocampal mossy fiber LTP. *Science.* 296:1864–1869.